SEMESTER PROJECT:

NANO-SAW DEVICES FOR RFID AND SENSING APPLICATION

STUDY OF THE LITHIUM NIOBATE BEHAVIOR

PROFESSOR: Guillermo Villanueva
SUPERVISOR: Andrea Lozzi
STUDENT: Seïfeddine Ben Khelil

December 2015

Content

Introduction 3
Passive RFID based on a SAW device 3
SAW devices 3
RFID principle 4
Final aim 4
Lithium Niobate 5
Crystal basis 5
Electromechanical coupling factor 5
Matrices of interest 6
Supplier's crystal cuts 7
Transformation of tensor constants 9
Results 9
Fabrication 11
Optimization of the photolithography 11
Results 12
Conclusion 13
MATLAB calculation 13
Fabrication 13
References 14
Appendix 15
Appendix 1: MATLAB main code “transform_2steps” 15
Appendix 2: MATLAB function “cut2euler” 18
Appendix 3: Transformation of tensor constants 19
Appendix 4: Process Flow 20
Appendix 5: Details on the process flow (runcard) 21
Appendix 6: Types of resists 22

Introduction

This project is the continuation of Kaitlin Howell's work in 2014 [1]. In that project all the components of an RFID based on a SAW device have been dimensioned and the process flow of the device has been established.

The key element of a SAW device is the piezoelectric material. The project aim is to increase our comprehension of the Lithium Niobate behavior. This material is anisotropic, thus, all the properties of the material are dependent of the orientation. Regarding to that, the crystal cut chosen for our device has strong consequences on its efficiency.

Passive RFID based on a SAW device

Radio-frequency identification (RFID) exploits electromagnetic fields to transfer data, for the purposes of automatically identifying and tracking tags attached to objects. Basically an RFID is a device which detects a radio-frequency signal and re-emits a secondary signal with a specific identification encoded.

SAW devices

Surface acoustic wave (SAW) devices have been studied since the 60s, starting with the conception of interdigital transducers on piezoelectric materials. SAW devices have been fabricated for a lot of applications including resonators, oscillators, bandpass filters and delay lines.

A simple SAW device is illustrated in figure 1: it is composed of two interdigital transducers that are fabricated by photolithography on a piezoelectric substrate. By applying a variable voltage on the input, the piezo-material generate mechanical deformation which propagate through the device. The opposite phenomena occurs in the output transducer and a voltage drop is created across the resistor.

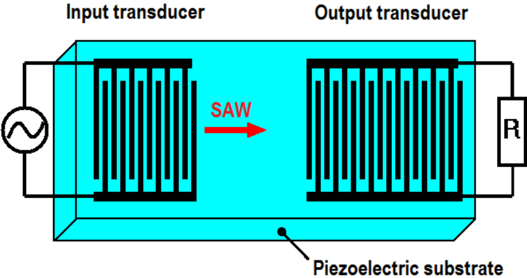

Figure 1: example of a SAW device

This type of IDT's (interdigital transducers) are designed for surface acoustic waves (depending on the excited mode). As shown on figure 2, in this configuration the intensity of the acoustic wave decays exponentially with the depth in the substrate, this is important and will be explained in the following paragraphs.

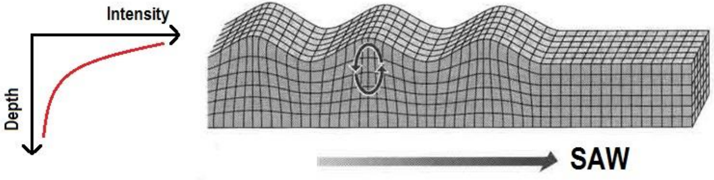

Figure 2: surface acoustic wave in the substrate

RFID principle

The principle of a RFID based on a SAW device is very close to the previous one. The output transducer is replaced by reflectors and an antenna is designed and linked to the input. In this configuration, an appropriate external RF signal can be detected by the antenna and gives rise to a surface acoustic wave. A reflected wave is produced by the reflectors, and since the whole process is reversible, a secondary signal is re-emitted by the antenna.

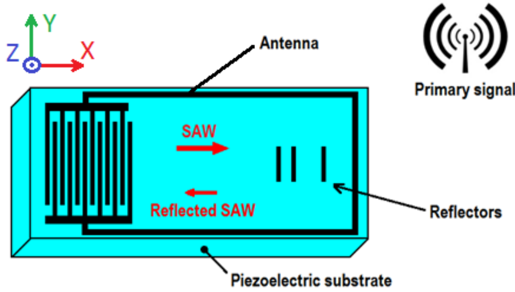

Figure 3: principle of RFID based on a SAW device

It is worth pointing out that:

1. The acoustic speed is much lower than the electro-magnetic wave (around 100 000 times lower). Because of that, a device of a few millimeter length can induce a delay of a few microseconds between the primary and the re-emitted signal. That makes possible the distinction of the two of them (figure 4).
2. The positioning of the reflectors generates a specific re-emitted signal depending on their spacing. For example, if we imagine a four bits code, the device of the figure 3 can be identified by the binary code 1101 (figure 4).

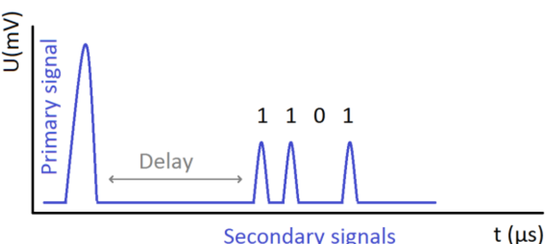

Figure 4: theoretical response of the RFID of the figure 3 to a RF pulse.
Graph of the measured signals by a sensor close to the device and the RF signal

Final aim

In a SAW device, all the energy of the acoustic wave is concentrated on the surface. The final device can be polished to a very thin layer (around 20 microns) so the RFID becomes flexible, that makes its integration with an object easier.

Since the device is small and passive, its efficiency need to be optimized, otherwise the secondary signal will be too low to be detected. The critical point is the capability of the material to convert an electric field to a mechanical deformation. This is called coupling factor of the piezoelectric material. The higher is the coupling factor the better is the efficiency of the conversion.

Lithium Niobate

Lithium Niobate ($LiNbO_3$) is a compound of niobium, lithium, and oxygen as shown in figure 5. Its single crystals are an important material for optical waveguides, piezoelectric sensors, optical modulators and various other applications. Crystals of lithium Niobate were first obtained in 1949 grown from a melt solution, at present, single-crystals Lithium Niobate are mainly grown in air by the Czochralski technique. The Lithium Niobate crystal is hexagonal and has three planes of symmetry. It is widely used in SAW device because of its very high coupling factor.

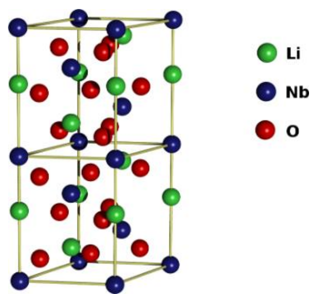

Figure 5: hexagonal unit cell of Lithium Niobate (LiNbO3)

Crystal basis

A hexagonal lattice is defined by four Miller-Bravais indices (a_1, a_2, a_3 and c). However to make the transformations easier it is needed to define an orthonormal basis in this system (figure 6). The X-axis is defined along a_1, the Z-axis along c and the Y-axis is defined with respect to the right hand rule [2].

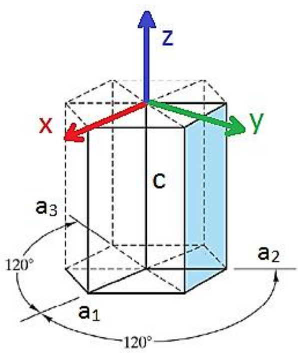

Figure 6: Miller-Bravais indices and the orthonormal basis

Electromechanical coupling factor

The electromechanical coupling factor, K indicates the effectiveness with which a piezoelectric material converts electrical energy into mechanical energy. The first subscript to K denotes the direction along which the electric field is applied; the second denotes the direction along which the mechanical energy is applied, or developed [3]. The following equation show K^2 as function of the electrical and mechanical properties of the material.

$$K_{xy}^2 = \frac{e_{xy}^2}{C_{yy}k_{xx}} \qquad \text{Equation 1}$$

e is the piezoelectric constant in [C/m^2], *C* is the elastic-stiffness constant in [Pa] and *k* the dielectric constant in [F/m].

A basis is defined so that the XY plane is on the surface of the device and the acoustic wave propagates along the X-axis. The Z-axis is perpendicular to the surface (figure 3).

In order to optimize the efficiency, the coupling factor is calculated in a very specific direction. In our device the electric field and the SAW propagation are oriented in the X-direction, but the stress in the material is a shear stress in the XZ plane. Thus with respect to equation 1 we can define the correct subscripts to the coupling factor.

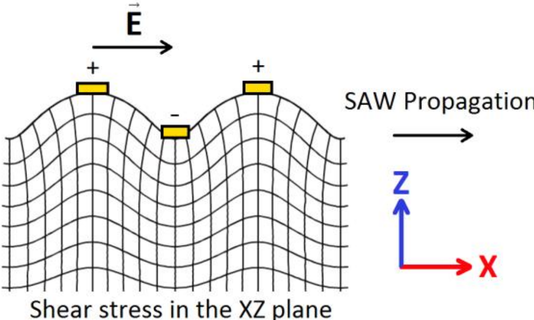

Figure 7: sectional view of the device around the IDTs

Matrices of interest

As explained in the previous section, three parameters are needed: the dielectric constant in the direction of the applied electric field, the compliance in the direction of the induced stress and the piezoelectric constant which links the two of them. These parameters come from the stress charge form of the piezoelectric constitutive equations:

$$T = C \cdot S + e^T \cdot E$$
$$D = e \cdot S + k \cdot E$$

S is the strain, *T* the stress in [Pa], *D* the electric displacement in [C/m^2] and *E* the electric field in [V/m]. The 3 properties of interest are tensors and depend on the material:

The elastic-stiffness matrix:

$$[C_{ij}] = \begin{bmatrix} C_{11} & C_{12} & C_{13} & C_{14} & 0 & 0 \\ C_{12} & C_{11} & C_{13} & -C_{14} & 0 & 0 \\ C_{13} & C_{13} & C_{33} & 0 & 0 & 0 \\ C_{14} & -C_{14} & 0 & C_{44} & 0 & 0 \\ 0 & 0 & 0 & 0 & C_{44} & C_{14} \\ 0 & 0 & 0 & 0 & C_{14} & C_{66} \end{bmatrix}$$

The piezoelectric matrix:

$$[e_{ijk}] = \begin{bmatrix} 0 & 0 & 0 & 0 & e_{15} & -e_{22} \\ -e_{22} & e_{22} & 0 & e_{15} & 0 & 0 \\ e_{31} & e_{31} & e_{33} & 0 & 0 & 0 \end{bmatrix}$$

The dielectric matrix:

$$[\kappa_{ij}] = \begin{bmatrix} \kappa_{11} & 0 & 0 \\ 0 & \kappa_{11} & 0 \\ 0 & 0 & \kappa_{33} \end{bmatrix}$$

Table 1: Elastic coefficients (GPa), piezoelectric coefficients (C/m²), and dielectric coefficients (pF/m)

C_{11}	C_{12}	C_{13}	C_{14}	C_{33}	C_{44}	e_{15}	e_{22}	e_{31}	e_{33}	k_{11}	k_{33}
199.5	55.27	67.67	8.7	235.2	59.48	3.65	2.39	0.31	1.72	398.9	232.2

All the values were obtained from the work of H. Ledbetter, N. Nobutomo and H. Ogi [4] wich compare their measurement with values from other papers.

In order to select the correct coefficient, it is important to understand how the subscripts of the tensors are organized. In Voigt notation the subscripts for a rank 4 tensor[1] are defined as:

$$\begin{bmatrix}\sigma_1\\\sigma_2\\\sigma_3\\\sigma_4\\\sigma_5\\\sigma_6\end{bmatrix} = \begin{bmatrix}C_{11} & C_{12} & C_{13} & C_{14} & C_{15} & C_{16}\\ C_{12} & C_{22} & C_{23} & C_{24} & C_{25} & C_{26}\\ C_{13} & C_{23} & C_{33} & C_{34} & C_{35} & C_{36}\\ C_{14} & C_{24} & C_{34} & C_{44} & C_{45} & C_{46}\\ C_{15} & C_{25} & C_{35} & C_{45} & C_{55} & C_{56}\\ C_{16} & C_{26} & C_{36} & C_{46} & C_{56} & C_{66}\end{bmatrix} \begin{bmatrix}\epsilon_1\\\epsilon_2\\\epsilon_3\\\epsilon_4\\\epsilon_5\\\epsilon_6\end{bmatrix}$$

With, XX=1, YY=2, ZZ=3, ZY=YZ=4, XZ=ZX=5 and XY=YX=6.

For example that means that the coefficient C_{24} links the stress in the direction YY to the deformation in the plane ZY (a square in the ZY plane is turned to a rhomboid). Thus C_{55} links the shear stress in the plane XZ to the deformation of the plane XZ.

For a rank 3 tensor[2] the first subscript does not change from a rank 4 tensor, but the second one goes from 1 to 3 with, X=1, Y=2 and Z=3,.

For a rank 2 tensor[3], both subscripts go from 1 to 3.

From that, we can define which coefficient is important for this application:

- The electric field is applied in the X direction thus k_{11} is needed.
- The stress is induced in the XZ plane thus C_{55} is needed.
- With respect to equation 1, the piezo-coefficient e_{15} makes the link.

With all that we can calculate the effectiveness of the conversion in our device which is $\boldsymbol{K_{15}^2}$.

Supplier's crystal cuts

Lithium Niobate can be purchased in different cuts. Since it is anisotropic, it is important to choose the best cut (with the higher coupling factor) for our application. For that we need to apply a transformation on all the tensors in order to calculate K_{15} for each cut.

In the previous sections we defined the crystal basis and the device basis. To be able to do the tensor transformation, Euler's angles are needed. Euler's angles are a set of three angles (φ, θ, Ψ) (figure 8) that describes the rotation from the device basis to the crystal basis.

φ is a rotation around the Z-axis.

θ is a rotation around the X'-axis. X' is the new X-axis after the rotation φ.

Ψ is a rotation around the Z''-axis. Z'' is the new Z-axis after both rotations (φ, θ).

[1] 6x6 matrix in Voigt notation.
[2] 6x3 matrix in Voigt notation.
[3] 3x3 matrix in Voigt notation.

Lithium Niobate suppliers does not use Euler's angles to define the orientation of their products. Designation like "X-cut $LiNbO_3$" or "YX 128° $LiNbO_3$" are widely used. Basically a crystal can be rotated 3 times before the cut [2, p. 1387] but this is never used by the suppliers, only single rotated ones are described in this section.

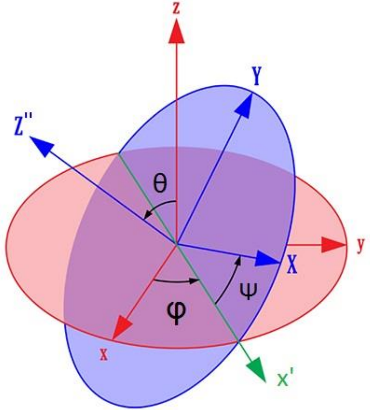

Figure 8: Euler's angles

All the single rotated cuts can be separated in 2 sections:

1. One axis designation

These three specific cuts are straightforward; X-cut, Y-cut and Z-cut. The axis in the designation is perpendicular to the surface. That means that the Z-cut makes the crystal basis and the device basis collinear.

2. Two axis designation

In this case the first axis is the plane[4] of the cut rotated[5] around the second axis by the specified angle. If we take as example XZ 30° Lithium Niobate: the plane defined by the X axis (YZ plane) is rotated by 30° around the Z-axis (figure 9).

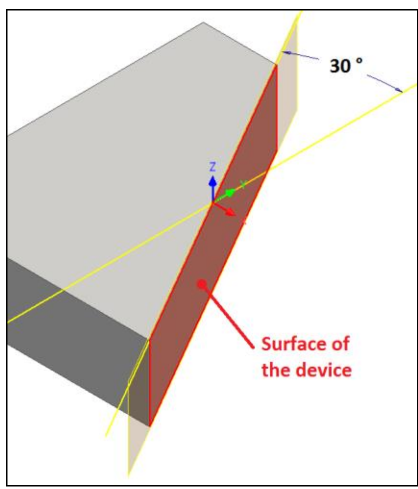

Figure 9: XZ 30° Cut.

[4] Each axis define the plane perpendicular to it. X-axis for the YZ plane, Y-axis for XZ plane and Z axis for the YX plane.
[5] Counter clockwise.

Knowing all that we can translate supplier's designation to Euler's angle for single rotated cuts:

Table 2: transformation of the suppliers cut to Euler's angles

Euler's angles (°)	X-cut	Y-cut	Z-cut	XY α°	XZ α°	YX α°	YZ α°	ZX α°	ZY α°
φ	0	0	0	0	0	0	0	0	0
θ	90	90	0	90+α	90	α-90	90	-α	α
ψ	90	0	0	90	90-α	0	-α	0	90

Transformation of tensor constants

Four different cuts have been compared in this project; X-cut, Y-cut, Z-cut and YX 128° $LiNbO_3$. A MATLAB code[6] has been implemented to calculate all the new tensor constant after rotation. More details on the software are in the appendix 3 [5].

A dedicated function[7] calculates the Euler's angles from the suppliers' cut as shown in the table 2. The coefficient of interest (C_{55}, e_{15} and k_{11} in our case) are specified as characters in the variable "data". It is possible to add as much coefficient as needed. All the graphics and the data will be automatically saved in different files (lines 126 to 177).

The code is split in two parts: in the first one, all the tensors are defined (lines 16 to 46) [4], then, using Euler's angles the tensors are modified to match a given orientation (lines 49 to 80).

In order to define which SAW propagation direction offers the higher coupling factor in a specific cut, the second part of the code rotates the sample around the axe perpendicular to the new surface of the sample (lines 90 to 124). The sample is rotated by 180° (this parameters can be modified at the line 12) and the tensors are calculated every degree (the step can be modified in line 13).

Results

All the values for the different coefficients are saved in three different Excel files (one for each cut), they're plotted together and K_{15}^2 (equation 1) is calculated directly in a new Excel document.

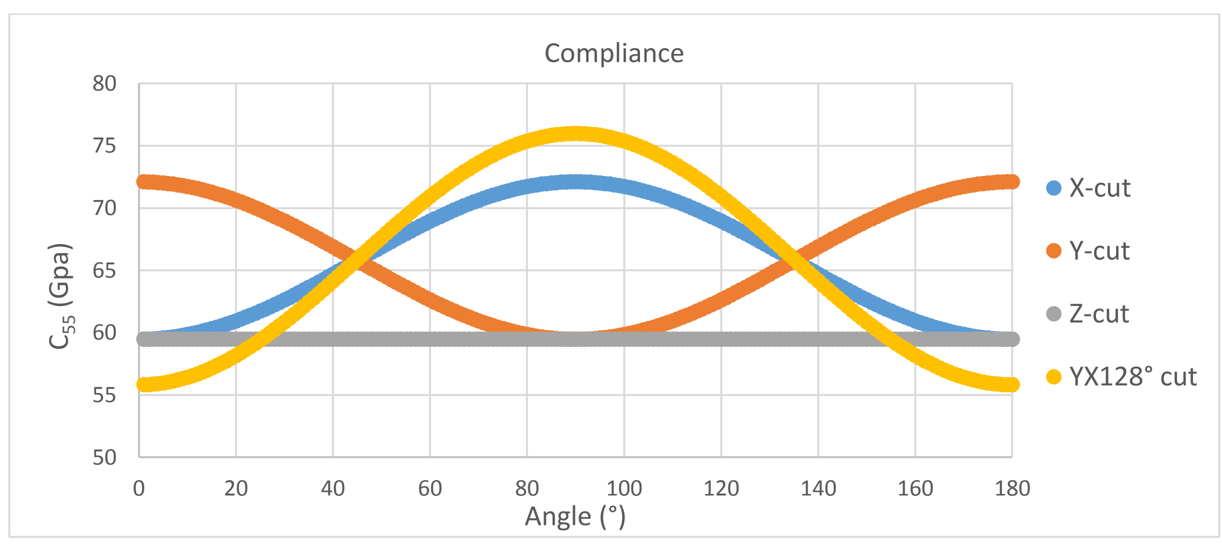

Figure 10: compliance VS propagation direction

[6] Appendix 1
[7] Appendix 2

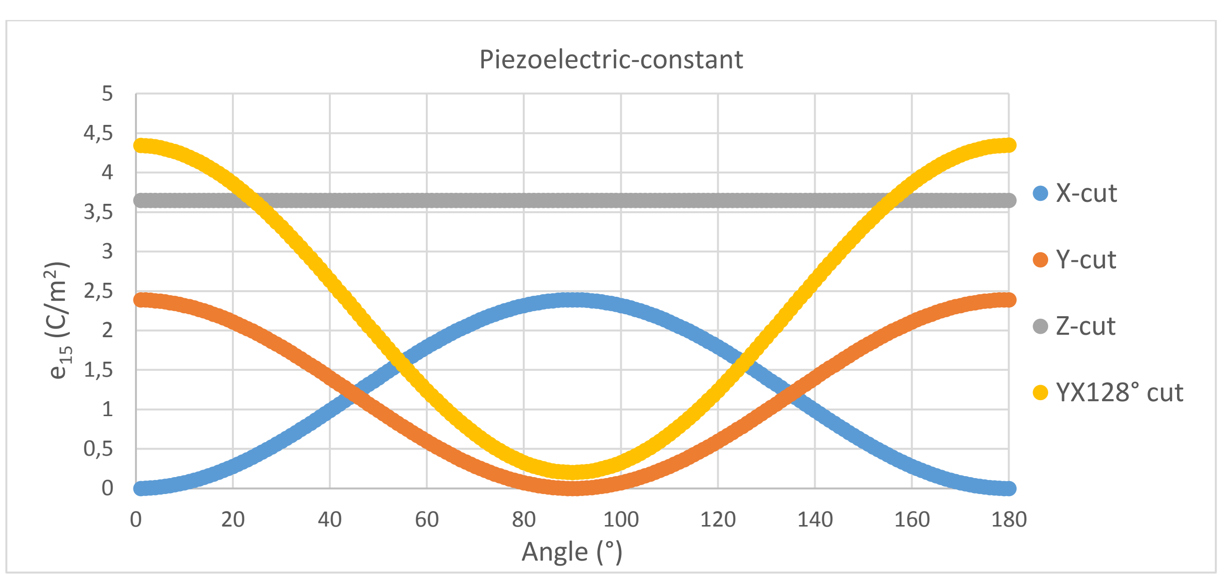

Figure 11:piezoelectric constant VS propagation direction

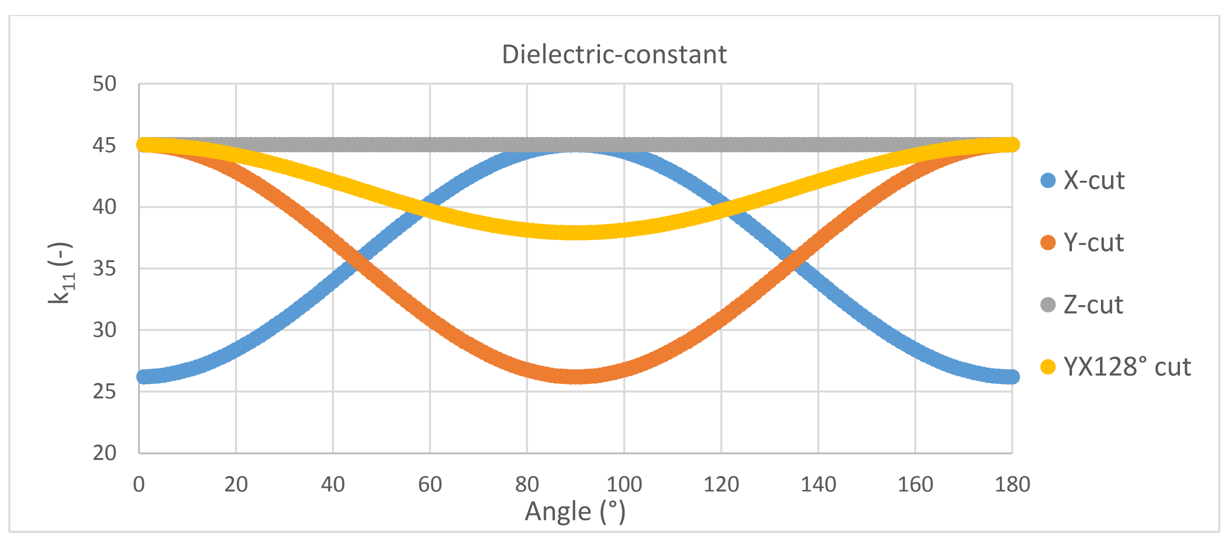

Figure 12: dielectric constant VS propagation direction

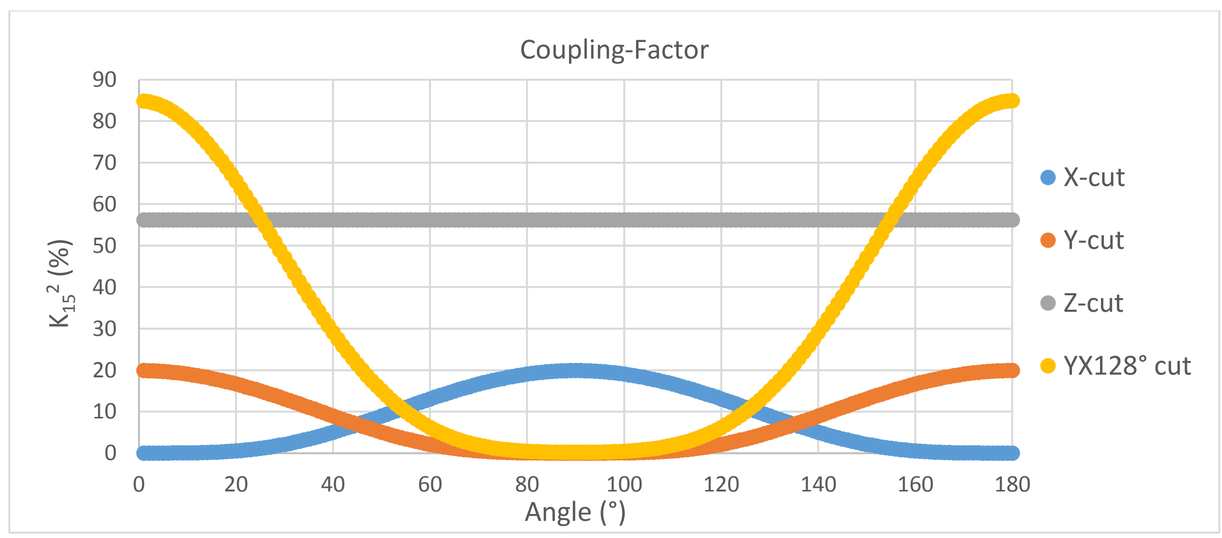

Figure 13: coupling factor VS propagation direction

Fabrication

The device is elaborated by photolithography and metallic deposition on the surface of a Lithium Niobate chip. At the beginning of this project the process flow (Appendix 4), which describes the steps of fabrication in the clean room was already established. A test mask (figure 14) for the photolithography had been elaborated in order to run some preliminary measures. The mask has several devices disposed in different orientations in order to measure the response as function of the propagation direction. The distance between the reflectors (upper pattern in the first zoom-in on the figure 14) and the IDTs is different in some devices on the mask that makes possible the characterization of the delay line. Moreover bonding pads are connected to the interdigital transducers (IDTs are shown in the second zoom-in on the figure 14) to facilitate the measures.

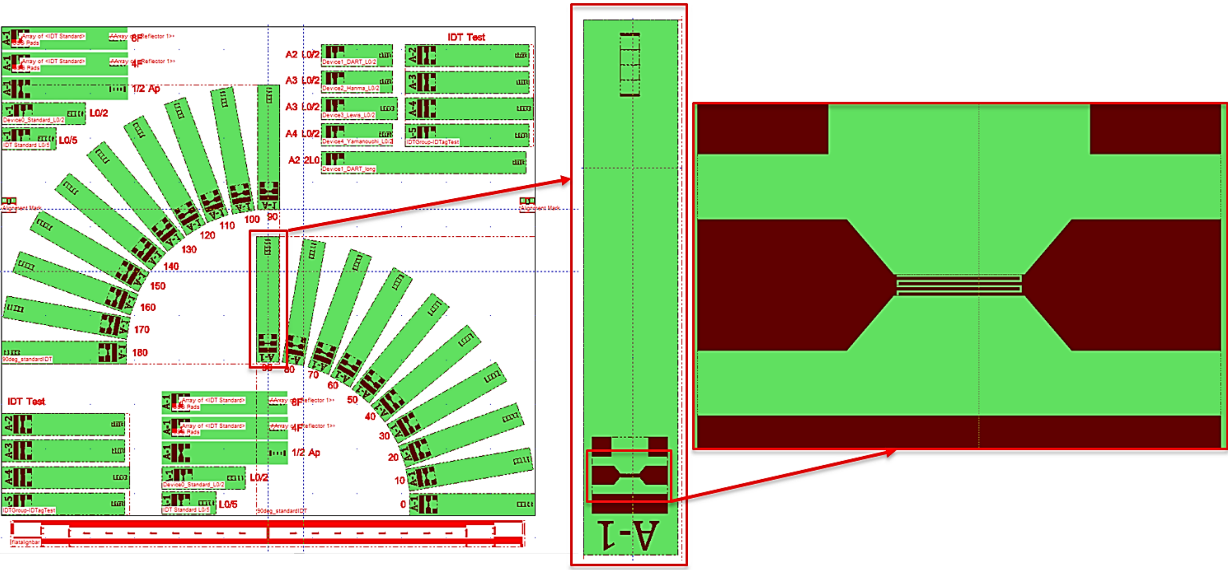

Figure 14: test masks with bonding pads and several orientations

Optimization of the photolithography

The parameters used in the previous project (Kaitlin Howell's work) needed to be updated since the material in the clean room has been modified, especially for the photolithography parameters. The first step of the fabrication consists in gluing the chip of lithium Niobate (14x15 mm^2) on a wafer of 100 millimeters. This operation is needed because all the systems in the cleanroom are designed to use wafers of 100 or 150 millimeters. The next step is the photolithography which is described in details in the appendix 5.

The resist used for the photolithography is a reversal resist (details in appendix 6). This type of resist need to be baked after exposure. The time and the temperature of this reversal baking can influence the quality of the pattern after development. To optimize the process all parameters related to the bake or the exposure can be modified. In order to minimize the number of tests (Lithium Niobate chips are expensive) the reversal baking has been fixed at 110° for 90 seconds and the exposure time has been tested at 4 different times. All the exposures were done on the same chip, this procedure was realized on a manual mask aligner (figure 15) with a cover on the mask.

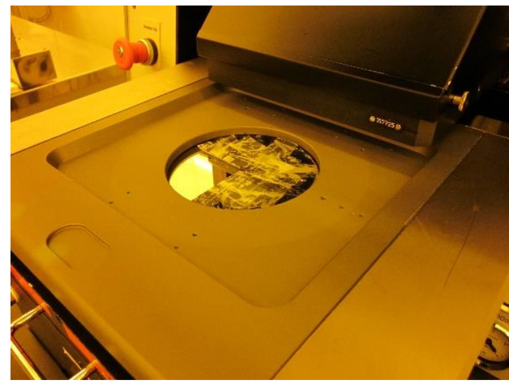

Figure 15: cover on the mask for the exposure test

The figure 16 describe how the exposures have been done on the Lithium Niobate chip. Three quarter of the mask are covered with a black sheet of paper. First of all the mask is aligned in the bottom left corner of the chip and exposed for 3 seconds at 10 mW/cm^2. The second exposure of 5 seconds is done after moving to the bottom right corner (the mask is moved by 7 mm to the right). The third exposure lasts 8 seconds after moving up by 7 mm, and the last one is an exposure of 11 seconds at the top left of the chip (the mask is moved by 7 mm to the left). If this procedure is properly done, there is no area double exposed on the resist.

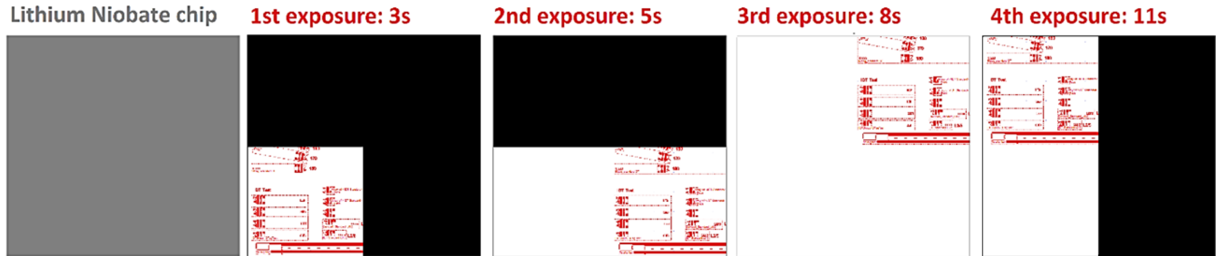

Figure 16: procedure of exposures for the multiple tests on the same chip.
In black the sheet of paper covering the mask and in red the design of the mask.

Results

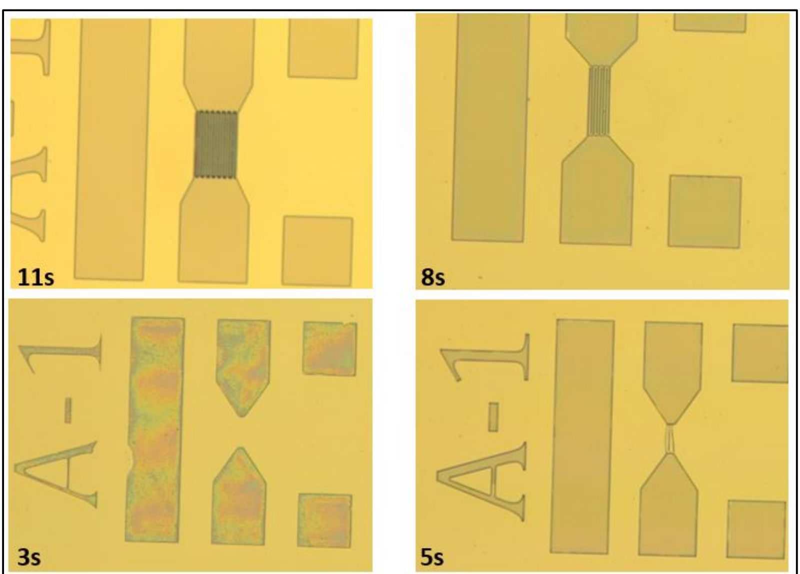

Figure 17: Image of the four exposures test under the microscope

After development with the parameters of the runcard (Appendix 5) and cleaning, the chip has been measured under the microscope.

The interdigital transducer did not appear properly for the first 2 exposures (3 and 5 seconds). However the pattern for the 8 and 11 seconds exposure looks good under the microscope as shown in the figure 17.

As shown on the figure 18, the dimension of the interdigital transducer (2 µm) which is the smallest dimension on the mask is almost reached with an exposure time of 11 seconds.

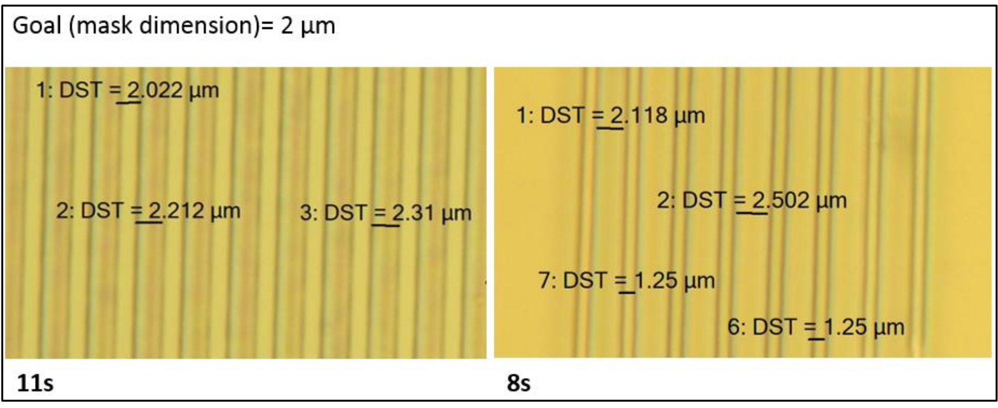

Figure 18: measurement of the IDTs dimensions after photolithography for 8 and 11 seconds exposures

Conclusion

MATLAB calculation

After the correction of the typo in the paper of A. H. Fahmy and E. L. Alder [5] (Appendix 3) all the calculated values seem correct. The compliance, the piezoelectric and the dielectric matrix can be calculated for any orientation of Lithium Niobate. This MATLAB code can be used to predict $LiNbO_3$ properties as function of the crystal cut. Specific coefficient can be extracted, plotted and saved in an Excel file. However properties like the coupling factor are not calculated in the MATLAB code but afterward in the Excel file.

The values seem correct with respect to the crystal symettry and the order of the magnitude. Moreover the YX 128° $LiNbO_3$ is the most widely used in the field of SAW devices, therefore the results makes sense since the coupling factor is up to 85% for this cut.

Nevertheless, all these results have to be validated by another way. Measurements on Lithium Niobate in several directions (every 10 degrees on 180 degrees for example) or/and a simulation on COMSOL should confirm what was obtained during this project.

Fabrication

The fabrication of the device did not go as far as scheduled because of unexpected problems. Only the first two steps of fabrication have been done. The gluing of the chip on the wafer and the photolithography worked well with the final parameters: reversal baking 90 second at 110° and exposure of 11 seconds at 10 mW/cm^2.

These parameters were tried one single time, a repeatability test should be ran to assure the quality of the next samples. Since the lithium Niobate is glued on the silicon and the reversal baking is done on a hot plate, it is possible that the reversal baking will not work every time because of thermal exchange problems. In this case, a reversal baking in an oven could improve the thermal exchange, but the baking time will be longer. In the end, all the final steps of the fabrication still need to be tested and optimized.

References

[1] K. Howell and P. G. Villanueva, "Nano SAW devices for sensing applications".

[2] PROCEEDINGS OF THE I.R.E, Standards on PIEZOELECTRIC CRYSTALS, 1949.

[3] American National Standards Institute, IEEE Standard on Piezoelectricity, 1987.

[4] H. Ledbetter, N. Nobutomo and H. Ogi, Elastic, anelastic, piezoelectric coefficients of monocrystal lithium niobate.

[5] A. H. Fahmy and E. L. Alder, Transformation of tensor constants of an anisotropic materials due to rotations of the co-ordinate axes.

[6] K.-y. Hashimoto, Surface Acoustic Wave Devices in Telecommunications.

Appendix

Appendix 1: MATLAB main code “transform_2steps”

```
close all
clear all
clc

%choose the crystal cut
PLAN='y';
AXE='x';
ANGLE=128;
data = ['C11';'e31';'k33'];
components = cellstr(data);

FA=180;             %final angle
step=1;             %steps between angles

%independant coeff.
eps0=8.854;
C11=199.5;
C12=55.27;
C13=67.67;
C14=8.7;
C33=235.2;
C44=59.48; %Gpa
e15=3.65;
e22=2.39;
e31=0.31;
e33=1.72;%C/m^2
k11=398.9/eps0;
k33=232/eps0; %[-]

C66=(C11-C12)/2;

C=[C11 C12 C13 C14 0 0;
   C12 C11 C13 -C14 0 0;
   C13 C13 C33 0 0 0;
   C14 -C14 0 C44 0 0;
   0 0 0 0 C44 C14;
   0 0 0 0 C14 C66];%elastic-stiffness matrix

e=[0 0 0 0 e15 -e22;
   -e22 e22 0 e15 0 0;
   e31 e31 e33 0 0 0];%piezoelectric matrix

k=[k11 0 0;
   0 k11 0;
   0 0 k33];%dielectric matrix

% first rotations for the cut

angles=cuts2euler(PLAN,AXE,ANGLE);

%euler's angles
phi=angles(1);     %rot Oz
tetha=angles(2);   %rot Ox'
psi=angles(3);     %rot Oz''

a1=cosd(psi)*cosd(phi)-cosd(tetha)*sind(phi)*sind(psi); %cos(x,x')
a2=-sind(psi)*cosd(phi)-cosd(tetha)*sind(phi)*cosd(psi);%cos(x,y')
a3=sind(tetha)*sind(phi);                               %cos(x,z')
b1=cosd(psi)*sind(phi)+cosd(tetha)*cosd(phi)*sind(psi); %cos(y,x')
b2=-sind(psi)*sind(phi)+cosd(tetha)*cosd(phi)*cosd(psi);%cos(y,y')
b3=-sind(tetha)*cosd(phi);                              %cos(y,z')
c1=sind(psi)*sind(tetha);                               %cos(z,x')
c2=cosd(psi)*sind(tetha);                               %cos(z,y') CORRECTED!
c3=cosd(tetha);                                         %cos(z,z')


V=[a1 b1 c1;
   a2 b2 c2;
   a3 b3 c3];
```

```
Q=[a1^2 b1^2 c1^2 2*b1*c1 2*c1*a1 2*a1*b1;
   a2^2 b2^2 c2^2 2*b2*c2 2*c2*a2 2*a2*b2;
   a3^2 b3^2 c3^2 2*b3*c3 2*c3*a3 2*a3*b3;
   a2*a3 b2*b3 c2*c3 b2*c3+b3*c2 c2*a3+c3*a2 a2*b3+a3*b2;
   a3*a1 b3*b1 c3*c1 b1*c3+b3*c1 c1*a3+c3*a1 a1*b3+a3*b1;
   a1*a2 b1*b2 c1*c2 b1*c2+b2*c1 c1*a2+c2*a1 a1*b2+a2*b1];

Cfc=Q*C*Q';
efc=V*e*Q';
kfc=V*k*V';


% second rotation after the cut (to decide of the direction of propagation)


t=0;
phi=0;
tetha=0;
psi=0;

for i=step:step:FA %automatic

t=t+1;

%euler's angles
phi=i;    %rot around the axe perpendicular to the surface


a1=cosd(psi)*cosd(phi)-cosd(tetha)*sind(phi)*sind(psi); %cos(x,x')
a2=-sind(psi)*cosd(phi)-cosd(tetha)*sind(phi)*cosd(psi);%cos(x,y')
a3=sind(tetha)*sind(phi);                               %cos(x,z')
b1=cosd(psi)*sind(phi)+cosd(tetha)*cosd(phi)*sind(psi); %cos(y,x')
b2=-sind(psi)*sind(phi)+cosd(tetha)*cosd(phi)*cosd(psi);%cos(y,y')
b3=-sind(tetha)*cosd(phi);                              %cos(y,z')
c1=sind(psi)*sind(tetha);                               %cos(z,x')
c2=cosd(phi)*sind(tetha);                               %cos(z,y')
c3=cosd(tetha);                                         %cos(z,z')

V=[a1 b1 c1;
   a2 b2 c2;
   a3 b3 c3];

Q=[a1^2 b1^2 c1^2 2*b1*c1 2*c1*a1 2*a1*b1;
   a2^2 b2^2 c2^2 2*b2*c2 2*c2*a2 2*a2*b2;
   a3^2 b3^2 c3^2 2*b3*c3 2*c3*a3 2*a3*b3;
   a2*a3 b2*b3 c2*c3 b2*c3+b3*c2 c2*a3+c3*a2 a2*b3+a3*b2;
   a3*a1 b3*b1 c3*c1 b1*c3+b3*c1 c1*a3+c3*a1 a1*b3+a3*b1;
   a1*a2 b1*b2 c1*c2 b1*c2+b2*c1 c1*a2+c2*a1 a1*b2+a2*b1];

Cf(:,:,t)=Q*Cfc*Q';
ef(:,:,t)=V*efc*Q';
kf(:,:,t)=V*kfc*V';
ang(t)=i;

end



FCOMP=size(components);

for h=1:1:FCOMP(1)
    t=0;
    component=components{h};

        for j=step:step:FA %loop to extract the values of the choosed component
            t=t+1;

            matrix1=component(1);
            matrixf=[matrix1,'f'];matrix=eval(matrixf);
            index1=component(2);
            index2=component(3);
            Yaxelabel=sprintf('%s%s%s',matrix1,index1,index2);
            index1=str2num(index1);
            index2=str2num(index2);

            comp(t)=matrix(index1,index2,t);
```

```
        end

        switch matrix1 %selection of the units for Y axis
            case 'C'
            units='Gpa';
            case 'e'
            units='C/m^2';
            case 'k'
            units='-';
        end

%plot the figure
figure(h)
plot(ang,comp,'LineWidth',2)
title( sprintf('%s%s %s° Lithium
Niobate',PLAN,AXE,num2str(ANGLE)),'FontSize',15,'FontWeight','bold' );
xlabel('Orientation (°)','FontSize',15,'FontWeight','bold')
ylabel(sprintf('%s (%s)',Yaxelabel,units),'FontSize',15,'FontWeight','bold','Color','r');
%save automatically the fig
saveas(h,sprintf('%s%s%s_%s.jpg',PLAN,AXE,num2str(ANGLE),Yaxelabel));

%create the excel file
lim=num2str((FA/step)+1);
range=h+1;
col = char(range+'A'-1);
column=sprintf('%s2:%s%s',col,col,lim);
tit=sprintf('%s%s_%s.xlsx',PLAN,AXE,num2str(ANGLE));
xlswrite(tit, comp', column);

end

rangefA=sprintf('A:A%s',lim); %write the angles in excel
xlswrite(tit, ang', 'A2:A181');
```

Appendix 2: MATLAB function “cut2euler”

```
function Euler_angles = cuts2euler(plan,axe,angle)

%this fonction transform the suppliers standards to euler's angles
% for example: YX 128° lithium niobate
%               plan='y', axe='x',angle=128
%               euler's angles are [0,38,0]
%for simple cut (X cut)
%               plan='x',axe'x',angle=0

% the variables plan and axe are single lowercase character(x,y or z)!!!!!
% angle is a number
%
% Example:          cuts2euler('y','x',128)
%
%                   ans =
%
%                         0    38     0


phi=0;
tetha=0;
psi=0;

    switch plan
    case 'x'
            switch axe
            case 'x'
            phi=0;tetha=90;psi=90;
            case 'y'
            phi=0;tetha=90+angle;psi=90;
            case 'z'
            phi=0;tetha=90;psi=90-angle;
            end
    case 'y'
            switch axe
            case 'x'
            phi=0;tetha=angle-90;psi=0;
            case 'y'
            phi=0;tetha=90;psi=0;
            case 'z'
            phi=0;tetha=90;psi=-angle;
            end
    case 'z'
            switch axe
            case 'x'
            phi=0;tetha=-angle;psi=0;
            case 'y'
            phi=0;tetha=angle;psi=90;
            case 'z'
            phi=0;tetha=0;psi=0;
            end
    end

Euler_angles=[phi,tetha,psi];

end
```

Appendix 3: Transformation of tensor constants

Indexing terms: *Computational physics, Elasticity, Permittivity, Piezoelectricity*

Abstract

The program package described in the paper performs the transformation of the stiffness, piezoelectric and permittivity (or conductivity) matrices of an anisotropic material under a rotation of the co-ordinate system.

1 Description of problem

If the constants in the system x, y and z are known and it is required to determine the constants in the new system x', y' and z' for which the orientation with respect to the first system is given by the Euler angles[1] ϕ, θ and ψ, the transformation matrix V is given by

$V =$ (1)

$\cos\psi\cos\phi - \cos\theta\sin\phi\sin\psi$	$\cos\psi\sin\phi + \cos\theta\cos\phi\sin\psi$	$\sin\psi\sin\theta$
$-\sin\psi\cos\phi - \cos\theta\sin\phi\cos\psi$	$-\sin\psi\sin\phi + \cos\theta\cos\phi\cos\psi$	$\cos\phi\sin\theta$
$\sin\theta\sin\phi$	$-\sin\theta\cos\phi$	$\cos\theta$

A mistake has been found in the paper used for the tensor transformation:

cos ϕ sin θ should be **cos Ψ sin θ**

which for compactness and generality is rewritten in terms of the direction cosines

$V =$ (2)

α_1	β_1	γ_1
α_2	β_2	γ_2
α_3	β_3	γ_3

where $\alpha_1 = \cos(x, x')$, $\gamma_2 = \cos(z, y')$ ... etc

The transformed stiffness, piezoelectric and permittivity constants for the rotated system are given in terms of the elements v_{ir} of the matrix V by

$$c'_{ijkl} = v_{ir} v_{js} v_{kt} v_{ln} c_{rstn} \quad (3)$$

$$e'_{ijk} = v_{ir} v_{js} v_{kt} e_{rst} \quad (4)$$

$$\epsilon'_{ij} = v_{ir} v_{js} \epsilon_{rs} \quad (5)$$

Two major disadvantages are hidden in eqns. 3 and 4, namely, the use of the tensor notation for c and e, and the huge number of multiplications required to compute the rotated constants. Typically, 1701 multiplication–addition operations are performed to compute the 21 different elastic constants, in addition to the necessary reindexing and storage requirements to convert from the fourth rank tensor notation to the matrix notation. One can simplify these formulas and convert to contracted index constants, thus saving both computing time and accuracy, by introducing the 6 x 6 matrix[2,3]

$Q =$ (6)

α_1^2	β_1^2	γ_1^2	$2\beta_1\gamma_1$	$2\gamma_1\alpha_1$	$2\alpha_1\beta_1$
α_2^2	β_2^2	γ_2^2	$2\beta_2\gamma_2$	$2\gamma_2\alpha_2$	$2\alpha_2\beta_2$
α_3^2	$\beta\phi$	γ_3^2	$2\beta_3\gamma_3$	$2\gamma_3\alpha_3$	$2\alpha_3\beta_3$
$\alpha_2\alpha_3$	$\beta_2\beta_3$	$\gamma_2\gamma_3$	$\beta_2\gamma_3 + \beta_3\gamma_2$	$\gamma_2\alpha_3 + \gamma_3\alpha_2$	$\alpha_2\beta_3 + \alpha_3\beta_2$

Using this matrix and its Q^t, the transformation formulas become

$$C' = QCQ^t \quad (7)$$

$$E' = VEQ^t \quad (8)$$

$$\epsilon' = V\epsilon V^t \quad (9)$$

where C, E and ϵ are the stiffness, piezoelectric and permittivity matrices $[c_{ij}]$, $[e_{ij}]$ and $[\epsilon_{ij}]$, respectively. Here, only 342 multiplication-addition operations are needed to compute the 21 different elastic constants, in contrast with 1701 operations for the previous method. In the simple case of a rotation in the xy plane around the z axis by an angle ψ, V and Q are obtained from eqns. 1 and 6 by substituting $\phi = \theta = 0$ which greatly simplifies the calculations.

Appendix 4: Process Flow

Technologies used			
Gluing, Mask fabrication, photolithography, positive resist, metal evaporation, lift-off, dry etching			
Photolith masks			
Mask #	**Critical Dimension**	**Critical Alignment**	**Remarks**
1	**1.2 um**	First Mask	Cr/Au Metallization
2	**2 um**	??	Dry Etching
Substrate Type			
XY-cut Lithium Niobate			

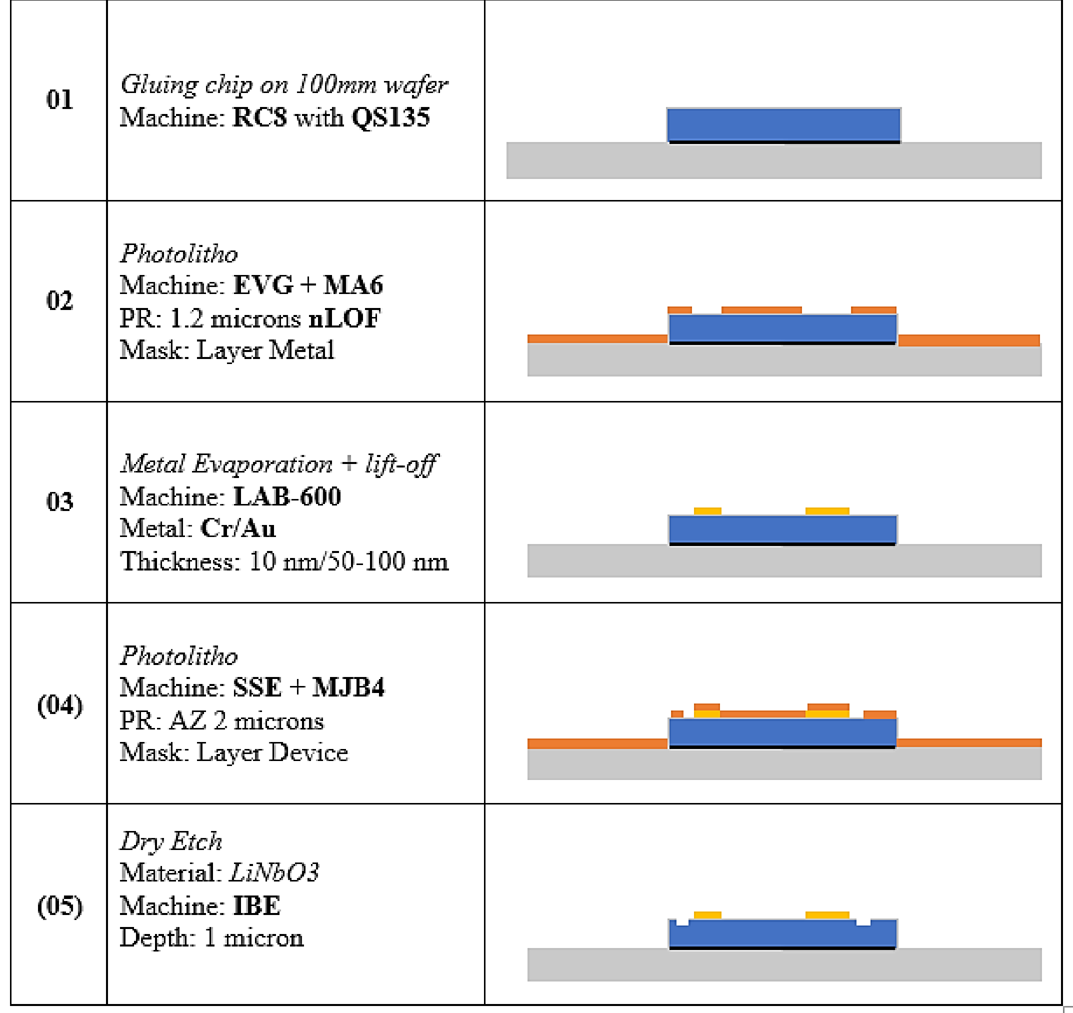

01	*Gluing chip on 100mm wafer* Machine: **RC8** with **QS135**	
02	*Photolitho* Machine: **EVG + MA6** PR: 1.2 microns **nLOF** Mask: Layer Metal	
03	*Metal Evaporation + lift-off* Machine: **LAB-600** Metal: **Cr/Au** Thickness: 10 nm/50-100 nm	
(04)	*Photolitho* Machine: **SSE + MJB4** PR: AZ 2 microns Mask: Layer Device	
(05)	*Dry Etch* Material: *LiNbO3* Machine: **IBE** Depth: 1 micron	

Appendix 5: Details on the process flow (runcard)

Project : SAW, Operator : Kaitlin Howell
Created : 30.04.2014 **Last revision** : 24.12.2015
Substrates : silicon <100>, 100mm, 525um, single side & LN chip, 1.4*1.5 cm^2

Step N°	Description	Equipement	Program / Parameters	Target	Actual	Remarks
0	**WAFER PREPARATION**					
0,1	Stock out					Si wafers, chips, mask
0,2	Check					
1	**GLUING**					
1,1	Prepare Equipment	Z6-Suess RC8 THP	Program 19			select program, check parameters
1,2	Secure Wafer	Z6-Suess RC8 THP	Program 19			Start program, load wafer
1,3	Apply Quick Stick/Chip	Z6-Suess RC8 THP	Program 19			Stop program, apply QS and chip
1,4	Finish Program	Z6-Suess RC8 THP	Program 19			Remove wafer, clean
2	**O2 PLASMA SURFACE CLEANING**					
2,1	Prepare Equipment	Z2/Tepla Gigabatch	Recipe descum, 30s			
2,2	Secure Wafer	Z2/Tepla Gigabatch	Recipe descum, 30s			Be careful with quartz carrier!
2,3	Program Run	Z2/Tepla Gigabatch	Recipe descum, 30s			
2,4	Finish Program	Z2/Tepla Gigabatch	Recipe descum, 30s			
3	**PHOTOLITHOGRAPHY - Mask 1**					
3,1	AZ nLOF 2000 coating	Z6/ EVG150	nLOF_No_dehydrated_1_4	1,4		
3,2	PR expose	Z6/Suess MA&BA6	First mask, HC, 10.0 mW/cm2			exposure time, ~11s
3,3	Developement	Z6/EVG150	DEV_no_dehydrated_1_4			
3,5	Inspection	Z6/uScope	Resolution and alignment			check w/ profilometer too
3,6	Relaxation	None	Wait 1 hr before further fab			
4	**O2 PLASMA SURFACE CLEANING**					
4,1	Prepare Equipment	Z2/Tepla Gigabatch	Recipe descum, 30s			
4,2	Secure Wafer	Z2/Tepla Gigabatch	Recipe descum, 30s			Be careful with quartz carrier!
4,3	Program Run	Z2/Tepla Gigabatch	Recipe descum, 30s			
4,4	Finish Program	Z2/Tepla Gigabatch	Recipe descum, 30s			Be careful, hot surface!
4	**METAL EVAPORATION**					
4,1	Cr Deposition	Z4/ LAB600H	HRN, 0.100 kA Cr	10 nm		Double check manual is off!
4,2	Au Deposition	Z4/ LAB600H	HRN, 0.500 kA Au	50 nm		
5	**LIFT-OFF**					
5,1	Prepare Equipment	Z14/Wet Bench	Glass tall containers			
5,3	LIFT-OFF	Z14/Wet Bench	SVC-14, 1 night			For inspection
5,4	Sink Rinse	Z14/Wet Bench	DI Rinse Sink			
5,5	Ultrasound	Z14/Wet Bench	25 minutes, 22C, power 1			Room T
5,6	Drying	Z14/Wet Bench	N2 gun			
5,7	Optical Inspection	Z14/ uScope				

Appendix 6: Types of resists

In general positive resists have a better resolution and edge quality relative to negative resists. However, negative resists normally have negative undercuts (after development) that make the lift-off easier compared to a positive undercut. By using an image reversal process, it is possible to take advantage of both attributes: the resolution of a positive resist and the undercuts of a negative one.